Solid State Sciences

Al
Al,Cr
Cr

Cr₅Al₈

Fe
Ga

FeGa

Ga
Si/Ga
Fe

Fe₆Ga₆₋ₓSi₁₊ₓ

First principles investigations of the hydrogenation effects on the electronic structure and the chemical bonding of CeIrAl

Samir F. Matar [a,*], Adel F. Al Alam [b,1], Michel Nakhl [c], Rainer Pöttgen [d], Bernard Chevalier [a], Naïm Ouaini [b]

[a] CNRS, Université de Bordeaux, ICMCB, 87 Avenue du Docteur Albert Schweitzer, 33600 Pessac, France
[b] Université Saint Esprit de Kaslik USEK, Faculté des Sciences, URA 'GREVE' (USEK/UL/CNRS), Jounieh, Lebanon
[c] Laboratoire de Chimie-Physique des Matériaux (LCPM), Université Libanaise, faculté des sciences II, Département de Chimie, Fanar, Lebanon
[d] Institut für Anorganische und Analytische Chemie, Universität Münster, Corrensstrasse 30, 48149 Münster, Germany

ARTICLE INFO

ABSTRACT

Hydrogenation of CeIrAl, leading to CeIrAlH$_2$, induces both changes of the crystal and electronic structure that we address within the density functional theory. The ab initio positioning of hydrogen leads to its coordination within Ce$_3$Ir tetrahedra and allows reproducing and interpreting the experimental findings of a Ce valence change from intermediate to trivalent in CeIrAlH$_2$ through the bonding of hydrogen with Ce and Ir. From Bader analysis of the charge density, hydrogen carries a charge of -0.39 and is found from energy differences to be weakly and covalently bonded in the intermetallic substructure. The results allow assessing the reversibility of hydrogen absorption/desorption in CeIrAl.

1. Introduction

Cerium based intermetallics have been widely studied in the last three decades with respect to their intriguing physical properties [1]. This is due to the peculiar valence behaviours, *i.e.* trivalent cerium has a [Xe]$4f^1$ configuration and exhibits paramagnetism (often accompanied by magnetic ordering), while tetravalent cerium, [Xe]$4f^0$, is diamagnetic. Various examples are known where the cerium valence can be influenced by temperature [2,3], by pressure [4], or upon hydrogenation [5,6].

Particularly, in the family of equiatomic CeTAl, for $T = $ Au and Pt, Ce is close to a stable trivalent state [7] while an intermediate-valence state for the Ce was evidenced in CeNiAl [8] and CeRuAl [9]. Hydrogenation of CeIrAl leads to a change of Ce from mixed-valent to trivalent with two hydrogen atoms per formula unit (fu) [10]. This is accompanied with a structural change from

orthorhombic (TiNiSi type, space group $Pnma$) to hexagonal (filled ZrBeSi type, space group $P6_3/mmc$). Table 1 shows the lattice parameters for both phases. There are twice more formula units in the orthorhombic structure of CeIrAl (Ce$_4$Ir$_4$Al$_4$) than in the hexagonal form of CeIrAlH$_2$ (Ce$_2$Ir$_2$Al$_2$H$_4$) then for comparing the volumes between 1 fu one has to divide the volumes by 4 and 2, respectively. The resulting volume expansion, $\Delta V/V = (69.8-59)/59 = 0.18$, is 18%. However the hydrogen positions were not determined experimentally. This involves strenuous deuteration for the purpose of neutron diffraction investigations. Nevertheless modern computation methodologies have revealed usefulness for searching the ground state configuration and properties. In order to examine the role played by hydrogen on the structural scale, such as the changes of the electronic structures and chemical bonding properties, we make the objective of determining the hydrogen sites in the intermetallic and examining the physico-chemical effects of its insertion into CeIrAl.

The structures of CeIrAl and CeIrAlH$_2$ are shown in Fig. 1. In the ternary intermetallic compound the iridium and aluminium atoms build up a three-dimensional, covalently bonded [IrAl] substructure in which the cerium atoms fill larger cavities. They are coordinated to two well ordered, but strongly puckered Ir$_3$Al$_3$ hexagons. Upon

Table 1
Calculated and experimental lattice parameters and atomic positions of a) CeIrAl and b) CeIrAlH$_2$ with Ce (2a) at 0, 0, 0; Ir (2c) at 1/3, 2/3, 1/4 and Al(2d) at 1/3, 2/3, 3/4 remaining unaltered after geometry optimization.

Pnma (No. 62); $Z = 4$	CeIrAl [10]	CeIrAl calc.
a)		
a-latt. param. (Å)	6.8954	6.903
b (Å)	4.3211	4.321
c (Å)	7.9411	7.941
Unit cell volume (Å^3)	236.61	236.86
Energy (eV)		−84.63
Atoms at 4c (x, 1/4, z)		
Ce (x, z)	0.9648, 0.8194	0.965, 0.819
Ir (x, z)	0.7339, 0.1160	0.734, 0.116
Al (x, z)	0.8640, 0.4304	0.864, 0.430
*P*6$_3$/*mmc* (No 194); $Z = 2$	CeIrAlH$_2$ [10]	CeIrAlH$_2$: H@4f
b)		
a-latt. param. (Å)	4.4012	4.427
c (Å)	8.3251	8.467
Unit cell volume (Å^3)	139.6	143.7
Energy (eV)		−56.272
H (4f) 1/3, 2/3, z	–	$z = 0.436$
Distances (Å)		
Ce−H		2.61
Ir−H		1.58
Al−H		2.95

hydrogen insertion, these hexagons become planar, similar to the boron-nitrogen network in hexagonal boron nitride. Consequently one observes a transition from a three- to a two-dimensional [IrAl] network. The bonding characteristics with hydrogen are discussed herein.

2. Computational details

The most appropriate quantum theoretical framework is the density functional theory DFT [11,12] within which we use two complementary computational methods. The Vienna ab initio simulation package (VASP) code [13] was first used to optimize the hydrogen coordinates and the binding energy of H in CeIrAl. For this we use projector augmented wave (PAW) potentials [14,15] built within the generalized gradient approximation (GGA) scheme [16]. The calculations were converged at an energy cut-off of 273 eV for the plane-wave basis set with respect to the k-point integration with a starting mesh of 4 × 4 × 4 up to 8 × 8 × 8 for best convergence and relaxation to zero strains. The Brillouin zone integrals were approximated using a special k-point sampling [15]. An analysis of the charge density is done with the approach of
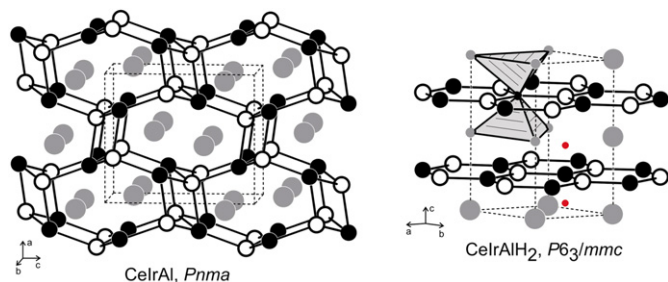

Fig. 1. The crystal structures of CeIrAl and CeIrAlH$_2$. Cerium, iridium, aluminium, and hydrogen atoms are drawn as medium grey, black filled, open, and small red circles, respectively. The three- and two-dimensional [IrAl] networks are emphasized. The H@Ce$_3$Ir tetrahedra are emphasized in the upper part of the CeIrAlH$_2$ structure. (For interpretation of the references to colour in this figure legend, the reader is referred to the web version of this article.)

"atoms in molecules and crystals" (AIM) introduced by Bader [17] who developed an intuitive way of dividing molecules into atoms as based purely on the electronic charge density. We use this criterion to evaluate the charge on H in the hydrogenated compound.

Then all-electron calculations, equally based on DFT with a GGA functional for the treatment of inter-electronic effects of exchange and correlation [16], are carried out with the optimized parameters for a full description of the electronic and chemical structures. They are performed using the full potential scalar-relativistic augmented spherical wave (ASW) method [18,19]. In the ASW method, the wave function is expanded in atom-centred augmented spherical waves, which are Hankel functions and numerical solutions of Schrödinger's equation, respectively, outside and inside the so-called augmentation spheres. In the minimal ASW basis set, we chose the outermost shells to represent the valence states and the matrix elements were constructed using partial waves up to $l_{max} + 1 = 4$ for Ce, *i.e.*, 4f(Ce) were considered within the basis set, $l_{max} + 1 = 3$ for Ir and Al and finally $l_{max} + 1 = 2$ for H. Self-consistency was achieved when charge transfers and energy changes between two successive cycles were such as: $\Delta Q < 10^{-8}$ and $\Delta E < 10^{-6}$ eV, respectively. The Brillouin zone integrations were performed using the linear tetrahedron method within the irreducible wedge [15]. The calculations are carried out assuming spin degenerate, non spin-polarized (NSP) configuration because experimentally both the intermetallic and the hydrogenated compound are not magnetically ordered at low temperature [10]. The relative magnitude of the chemical bonding is obtained based on the overlap population analysis: S_{ij}, i and j being two chemical species. The crystal orbital overlap population (COOP) criterion is used [20]. In the plots positive, negative and zero COOP magnitudes indicate bonding, anti-bonding and non-bonding interactions respectively.

3. Geometry optimization and binding energy

Starting from the lattice parameters and the Ce, Ir and Al atomic positions determined from X-ray powder diffraction data for CeIrAl and CeIrAlH$_2$ [10], a full geometry optimization was undertaken without any constrain on the shape (ISIF = 3 in VASP's INCAR). The CeIrAlH$_2$ structure, space group *P*6$_3$/*mmc*, contains two formula units per cell. With Ce (2a), Ir (2c) and Al (2d) found at two-fold atomic positions, two four-fold Wyckoff positions are available to insert hydrogen: 4e (0, 0, z') with the two hydrogen atoms aligned on the c axis between the Ce atoms and 4f (1/3, 2/3, z) with hydrogen located in a Ce$_3$Ir tetrahedral-like coordination (Fig. 1). Both hypotheses were considered in the calculations. Note that the other available 6-fold (6g, 6h) and 12-fold (12i, 12j, 12k) positions were not considered here for crystal chemical reasons, although compounds absorbing larger amounts of hydrogen such as Laves phases [21] show higher multiplicities for hydrogen sites. Starting z' and z parameters were chosen ad hoc to $z' = 0.3$ and $z = 0.4$.

Table 1 shows in two panels the basic crystallographic data of CeIrAl and CeIrAlH$_2$. A good agreement between experimental and calculated values is found for the lattice parameters and the coordinates in CeIrAl. For the hydride only one crystal chemically reasonable solution was obtained. A slightly larger calculated volume was obtained for the H@4f hypothesis with a final z value of 0.436. The second hypothesis (H@4e) had to be discarded because of a large energy destabilization directly related with much too short H−H distances of ∼0.8 Å.

As for the 4 Å^3 larger volume of the retained solution (H@4f), this is likely due to the use of the GGA functional of the DFT which usually leads to larger lattice spacing, *i. e.* it is 'under-binding' *versus* the homogeneous electron based LDA (local density

approximation) which is 'over-binding'. But since this volume difference is only observed in the hydride, another possibility might be that the measured experimental sample may be sub-stoichiometric with hydrogen, i.e. the hydrogen content could be slightly less than 2. Actually the hydrogenation of CeAuAl which undergoes the same structural transformation upon hydrogen uptake is only up to 1.4 H per fu [22]. Then it can be suggested that the pressure P_{H_2} used experimentally plays a major role in the saturation or not of the initial intermetallic with hydrogen.

Hydrogen on the $4f$ site with $z = 0.436$ is located in Ce_3Ir tetrahedra (Fig. 1) with d(Ce−H) = 2.61 Å and d(Ir−H) = 1.58 Å (Table 1b). The Al−H distance is much larger (∼2.95 Å) and leads to negligible Al−H bonding (vide infra). The electric charge carried by hydrogen is −0.39 electron as obtained from the analysis of the charge density with AIM theory [17]. This indicates covalently bonded hydrogen in CeIrAlH₂, contrary to ionic like hydrides such as MgH₂ where hydrogen carries a charge close to −1 [23]. Note that ionic hydrides are less easily envisaged for hydrogen storage/ release and require relatively high temperatures for their use (cf. [24] and therein cited works). Upon hydrogenation the changes are such that Ce becomes more electropositive 1.2 → 1.6 in accordance with its change of valence and its bonding with H; Ir which is the most electronegative becomes less negatively charged due to its bonding with hydrogen and −4.2 → −3.7 and Al which is the most electropositive does not change its charge, i.e. it remains 3+.

From the total energies (Table 1) one can deduce the binding of hydrogen in the hydride structure:

$$E_{bind.(H)} = E_{tot.}(CeIrAlH_2) - 1/2 E_{tot.}(CeIrAl) - 2 E_{tot.}(H_2)$$

$$\text{for two formula units.}$$

The third term of equality is derived from PAW-GGA calculations by placing dihydrogen in a cube box with a large lattice spacing of 5 Å. The resulting energy $E(H_2) = -6.59$ eV, is the total electronic energy. It includes twice the energy of mono-hydrogen (−0.95 eV from similar calculations), and it needs to be corrected by the zero point energy (ZPE). For H_2, ZPE amounts to ∼0.28 eV as calculated by the same method [25]. The binding energy of H_2 is then −4.41 eV which is close in magnitude to the dissociation energy (inverse sign) of the molecule as obtained from fluorescence excitation spectroscopy: ∼36118 cm^{-1}, i. e. ∼4.48 eV [26]. Then the stabilization energy of hydrogen in CeIrAlH₂ is −0.78 eV for 4 H or i.e. ∼−0.20 eV/H. This value indicates weakly bonded hydrogen in CeIrAlH₂, versus ionic hydrides for instance.

The feature of the relatively large volume change (18% experimentally; ∼20% from the calculations) is worth addressing as a support of the change of valence of cerium. This was observed experimentally for hydrogenated Ce based Laves phase $CeRu_2 \rightarrow CeRu_2H_4$ versus a normal rare earth, lanthanum ($LaRu_2 \rightarrow LaRu_2H_4$) [27]. To model such a situation in present study, Ce was replaced by La leading to hypothetic LaIrAl → LaIrAlH₂; then a full geometry optimization was carried out for the corresponding orthorhombic and hexagonal cells. The volume increase from LaIrAl to LaIrAlH₂ is then 12%. This lower magnitude of volume change (versus 18% in Ce compounds) can then be assigned only to the hydrogen uptake without change of valence for lanthanum upon hydrogenation, as one expects.

Lastly it was interesting to check whether the hexagonal structure of the hydride compound could be sustainable after hydrogen desorption. A full geometry optimization without the two hydrogen atoms led to a large energy destabilization with respect to the pristine CeIrAl experimental structure: −84.63 (CeIrAl space group $Pnma$) versus −76.57 eV (CeIrAlH₂ space group $P6_3/mmc$) and smaller volume of 212 Å³. This meets the experimental observation of the recovery of the orthorhombic structure after hydrogen

desorption [10] and implies that non puckered Ir_3Al_3 planar hexagons in the hexagonal hydride structure are destabilized in favour of strongly puckered hexagons (Fig. 1) of the orthorhombic structure of the pristine intermetallic, upon hydrogen departure.

4. Electronic structure and chemical bonding

4.1. Density of states

Using the optimized atomic positions (Table 1), we calculated the electronic band structures and the properties of chemical bonding with the full potential ASW method. The site projected density of states (PDOS) accounting for site multiplicities are given in Fig. 2. For the sake of clear presentation, the H partial PDOS are multiplied by 5 (Fig. 2b). In this panel as well as in the following ones, the zero energy is at the Fermi level (E_F).

Both compounds show three main energy regions for the PDOS. Within the valence band (VB), the Al s like states are present at low energy (−8 eV), then Ir d like states are found fully within the VB {−4, −2 eV} due to the large filling of its d subshell. On the opposite, only the lower part of Ce f states are crossed by E_F; the largest part of the Ce f states being found in the conduction band (CB) due to the presence of Ce at the beginning of the $4f$ series with a modestly occupied $4f$ shell. In the hydride the VB extends to lower energy, down to −9 eV and there is a larger localization of the d and f bands as a result of the increase of the interatomic distances in the expanded lattice. The DOS are mirrored by the band structure plotted in Fig. 3a which exhibit a continuous VB with large
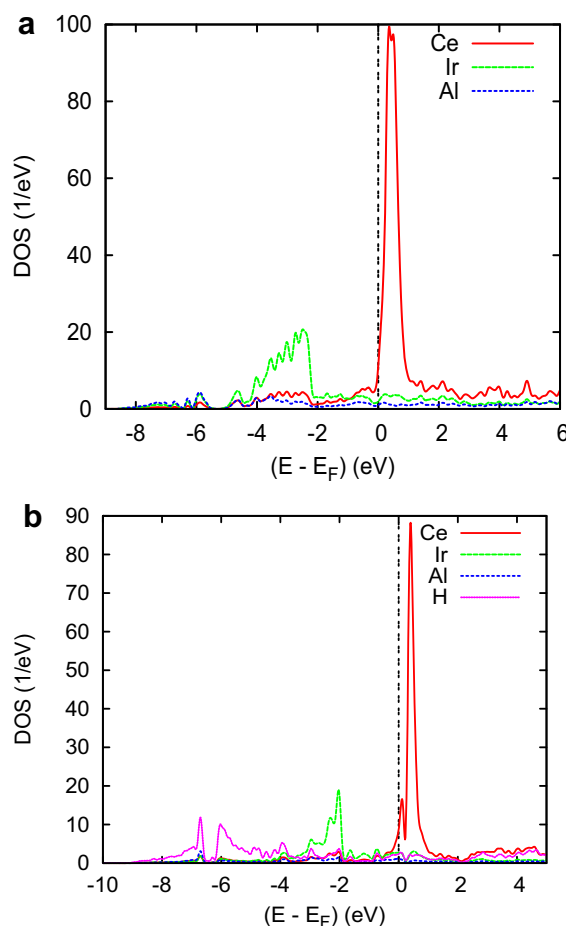

Fig. 2. Site projected density of states (PDOS) of (a) CeIrAl and (b) CeIrAlH₂. H PDOS are artificially enhanced five times for clarity.
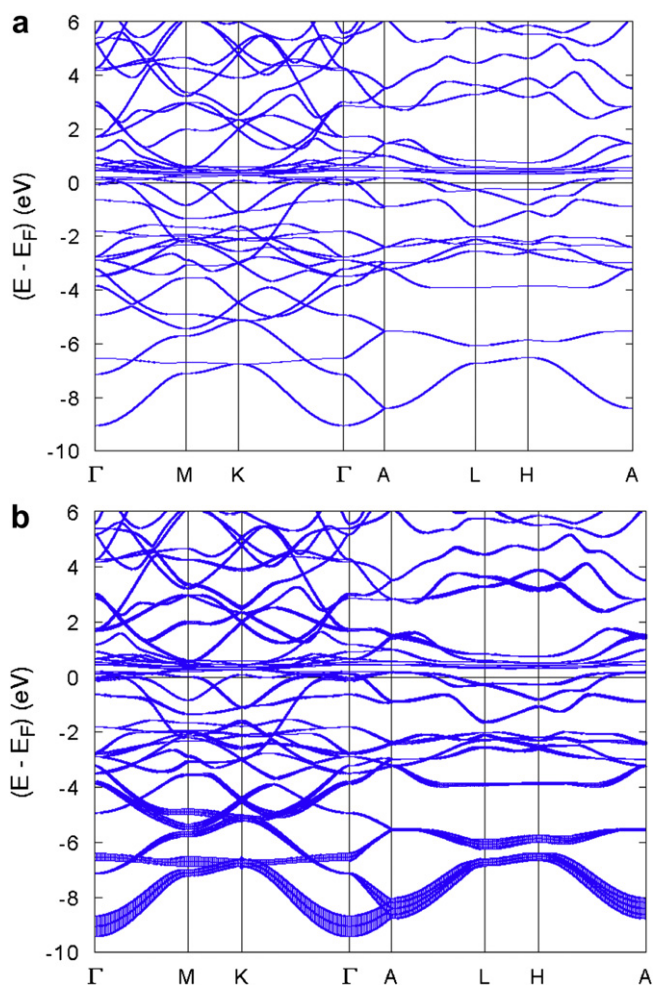
Fig. 3. (a) Band structure along the major lines of the hexagonal Brillouin zone of CeIrAlH$_2$ and (b) with hydrogen weighted bands. Fat (thick) bands signal large H contribution.

Fig. 4. Chemical bonding for hydrogen interactions with Ce, Ir and Al in CeIrAlH$_2$.

dispersive s,p like bands at the lower part and little dispersed bands (f like) around the Fermi level. The dispersion of d bands (−4, −2 eV) is intermediate. For an assessment of the extension of hydrogen states within the VB and CB, Fig. 3b shows the H weighted band structure of CeIrAlH$_2$. The largest contribution arising from H is at the lowest part of the VB from −10 to −6 eV as shown by the fat bands whose dispersion signals the s like states. However H is also found weighting bands in the region of the presence of Ir d states above −6 eV as well as around and above E$_F$ into the CB for Ce f flat bands (localized states). From this H s states are smeared over the energy range and signal a covalently bonded hydrogen.

Despite the localization of the Ce states in the hydride, the density of states at the Fermi level n(E$_F$) does not increase and remains around 10 states/eV for the 4f PDOS. This is contrary to the case of CeIrSb where nCe−CeIrSb(E$_F$) = 10 states/eV and nCe−CeIrSbH(E$_F$) = 38 states/eV [28]. In the Stoner mean field theory of band ferromagnetism [29] this indicates the stability of the compound and its hydrogenated homologue in a non magnetic NSP configuration in agreement with experiment [10]. On the contrary for CeIrSbH an ordered magnetic moment was found in agreement with experiment when spin polarization was allowed in SP calculations [28].

For rare earth elements belonging to the middle of the series, the degree of localization of f states becomes important and the treatment of itinerant as well as localized electrons within the same
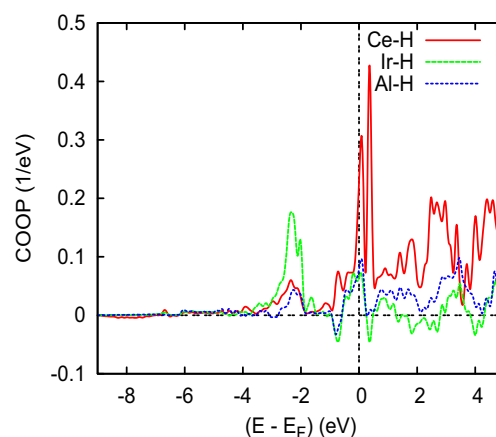
theoretical framework becomes difficult and imposes the use of self interaction corrections (SIC) which cancel the erroneous effects of the interaction of an electron with itself as obtained by the LDA/GGA XC schemes. But cerium is a particular rare earth (as well as uranium among actinides) and several compounds based on cerium (and uranium) are magnetically ordered at normal pressure. So it is admitted that their magnetism is of band type, i.e. it is mediated by the −inter atomic− electron gas, while for the other (normal) rare earths it is mainly of intra-atomic nature. Then the treatment at least qualitatively within a mean field theory (Stoner) can be of usefulness to their understanding. The question of the ratio: itinerant/localized f electrons in such rare earths/actinides is an open one.

4.2. Chemical bonding

The interactions of Ce, Ir and Al with H are shown in Fig. 4. The largest contributions are found for Ir−H. Despite the larger Ce−H distance (cf. Table 1b), the bonding of Ce with H is only of slightly lower magnitude than Ir−H due to the environment of H with three Ce and one Ir atom. Weakest interactions arise from Al−H due to their large separation. Then the major bonding is within the Ce$_3$Ir tetrahedron surrounding H with a larger Ir−H bonding due to the smaller interatomic distance versus Ce−H as shown in Table 1. Little bonding is found up to −4 eV and the main interactions with H occur between H itinerant (delocalized) states with Ir(d) and Ce(f). Note that some antibonding can be observed for Ir−H within the VB due to the already large filling of Ir d states so that extra electrons arising from hydrogen are found in antibonding states at ∼ −1 eV.

The emerging picture is that of two effects leading to the change of the Ce valence to trivalent:

(i) Hydrogen insertion leads to a large lattice expansion (versus a normal rare earth) and causes the Ce−Ce distance to increase from ∼3.6 Å to ∼4.2 Å. Then the f−f overlap between adjacent Ce atoms decreases. This features the broad, overlapping, Ce f states in CeIrAl (Fig. 2a) which become narrow and separated (non-overlapping) in CeIrAlH$_2$ (Fig. 2b).

(ii) The quantum mixing of the valence states of the metal constituents with H 'ligand' especially Ce as shown by the chemical bonding plots.

5. Conclusion

Finding atomic positions for hydrogen from ab initio calculations allowed examining the effect of the insertion of hydrogen into

S.F. Matar et al. / Solid State Sciences 13 (2011) 1704–1708

CeIrAl, which is found, among different hypotheses, most stable in a Ce_3Ir tetrahedral environment from full geometry optimization of the hydride structure. H is found to chemically bond to both Ce and Ir. These features may explain the transition from an intermediate-valence state to a trivalent state for Ce evidenced during the hydrogenation of CeIrAl. The results provided a good agreement with experiment for the lattice parameters and atomic positions of Ce, Ir and Al and led to identify weakly, covalently bonded hydrogen within the intermetallic structure with H −0.39 charge. These results allow explaining the observed absorption/desorption cycling. Further from the total energy differences we propose an assessment of the reformation of the orthorhombic intermetallic when H leaves the hexagonal structure which is then largely destabilized.

Acknowledgements

References

[1] A. Szytuła, J. Leciejewicz, Handbook of Crystal Structures and Magnetic Properties of Rare Earth Intermetallics. CRC Press, Boca Raton, 1994.
[2] T. Ueda, D. Honda, T. Shiromoto, N. Metoki, F. Honda, K. Kaneko, Y. Haga, T.D. Matsuda, T. Takeuchi, A. Thamizhavel, K. Sugiyama, K. Kindo, R. Settai, Y. Onuki, J. Phys. Soc. Jpn. 74 (2005) 2836.
[3] E. Gaudin, B. Chevalier, B. Heying, U.C. Rodewald, R. Pöttgen, Chem. Mater. 17 (2005) 2693.
[4] A. Jayaraman, W. Lowe, L.D. Longinotti, E. Bucher, Phys. Rev. Lett. 36 (1976) 366.
[5] B. Chevalier, R. Decourt, B. Heying, F.M. Schappacher, U.C. Rodewald, R.-D. Hoffmann, R. Pöttgen, R. Eger, A. Simon, Chem. Mater. 19 (2007) 28.
[6] S.F. Matar, Phys. Rev. B 75 (2007) 104422.
[7] D.T. Adroja, B.D. Rainford, L. Menon, S.K. Malik, J. Phys. Condens. Matter 9 (1997) 4743.
[8] J.-L. Bobet, B. Chevalier, B. Darriet, M. Nakhl, F. Weill, J. Etourneau, J. Alloys Compd. 317–318 (2001) 67.
[9] W. Hermes, S.F. Matar, R. Pöttgen, Z. Naturforsch. 64b (2009) 901.
[10] S.K. Malik, P. Raj, A. Sathyamoorthy, K. Shashikala, N. Narish Kumar, L. Menon, Phys. Rev. B 63 (2001) 172418.
[11] P. Hohenberg, W. Kohn, Phys. Rev. 136 (1964) B864.
[12] W. Kohn, L.J. Sham, Phys. Rev. 140 (1965) A1133.
[13] G. Kresse, J. Furthmüller, Phys. Rev. B 54 (1996) 11169.
[14] G. Kresse, J. Joubert, Phys. Rev. B 59 (1999) 1758.
[15] P.E. Blöchl, Phys. Rev. B 50 (1994) 17953.
[16] J. Perdew, K. Burke, M. Ernzerhof, Phys. Rev. Lett. 77 (1996) 3865.
[17] E. Sanville, S. Kenny, R. Smith, G. Henkelman, J. Comp. Chem. 28 (2007) 899 and a web ref. http://www.chemistry.mcmaster.ca/aim/aim_0.html.
[18] A.R. Williams, J. Kübler, C.D. Gelatt, Phys. Rev. B 19 (1979) 6094.
[19] V. Eyert, The Augmented Spherical Wave Method − A Comprehensive Treatment Lecture Notes in Physics. Springer, Heidelberg, 2007.
[20] R. Hoffmann, Angew. Chem. Int. Ed. Engl. 26 (1987) 846.
[21] V. Paul-Boncour, S.F. Matar, Phys. Rev. B 70 (2004) 184435.
[22] B. Chevalier, J.-L. Bobet, M.L. Kahn, F. Weill, J. Etourneau, J. Alloys Compd. 334 (2002) 20.
[23] S.F. Matar, Prog. Solid State Chem. 38 (2010) 1.
[24] S.F. Matar, M. Nakhl, A.F. Al Alam, M. Zakhour, N. Ouaini, Solid State Sci. 13 (2011) 569.
[25] O.I. Velikikhatnyi, P.N. Kumta, Mater. Sci. Eng. B. 140 (2007) 114.
[26] A. Balakrishnan, V. Smith, B.P. Stoicheff, Phys. Rev. Lett. 68 (1992) 2149.
[27] J. Osterwalder, T. Riesterer, L. Schlapach, F. Vaillant, D. Fruchart, Phys. Rev. B 31 (1985) 8311.
[28] S.F. Matar, E. Gaudin, B. Chevalier, R. Pöttgen, Solid State Sci. 13 (2011) 948.
[29] P. Mohn, Magnetism in the Solid State − an Introduction. Springer Series in Solid State Sciences. Springer, Heidelberg, 2003.